

1 **Production regime and associated N cycling in the vicinity**
2 **of Kerguelen Island, Southern Ocean**

3
4 **A.J. Cavagna¹, F. Fripiat¹, M. Elskens¹, P. Mangion², L. Chirurgien³, I. Closset⁴,**
5 **M. Lasbleiz³, L. Florez-Leiva^{5,6}, D. Cardinal⁴, K. Leblanc³, C. Fernandez⁷⁻⁸, D.**
6 **Lefèvre³, L. Oriol⁸, S. Blain⁸, B. Quéguiner³ and F. Dehairs¹**

7
8 [1]{Analytical, Environmental and Geo-Chemistry dept. (AMGC), Earth System Sciences
9 Research Group, Vrije Universiteit Brussel, Brussels, Belgium}

10 [2]{Centre for Coastal Biogeochemistry Research, Southern Cross University, Lismore,
11 Australia}

12 [3]{Aix-Marseille Université, Université de Toulon, CNRS/INSU, IRD, MIO, UM 110,
13 13288, Marseille, CEDEX 09, France}

14 [4]{Sorbonne Universités (UPMC, Univ Paris 06)-CNRS-IRD-MNHN, LOCEAN
15 Laboratory, 4 place Jussieu, F-75005 Paris, France}

16 [5]{Program of Oceanography, University of Antioquia, Medellin, Colombia}

17 [6]{Program of Biology, University of Magdalena, Santa Marta, Colombia}

18 [7]{Department of Oceanography, COPAS SurAustral program and Interdisciplinary Center
19 for Aquaculture Research (INCAR), University of Concepción, Chile}

20 [8]{Sorbonne Universités, UPMC Université Paris 06, UMR 7621, Laboratoire
21 d'Océanographie Microbienne, Observatoire Océanologique, F-66650 Banyuls/mer, France}

22
23 Correspondence to: acavagna@vub.ac.be

28 **Abstract**

29 Although the Southern Ocean is considered a High Nutrient Low Chlorophyll (HNLC) area,
30 massive and recurrent blooms are observed over and downstream of the Kerguelen Plateau.
31 This mosaic of blooms is triggered by a higher iron supply resulting from the interaction
32 between the Antarctic Circumpolar Current and the local bathymetry. Net primary production,
33 N-uptake (NO_3^- and NH_4^+), and nitrification rates were measured at 8 stations in austral spring
34 2011 (October-November) during the KEOPS 2 cruise in the Kerguelen Plateau area. Natural
35 iron fertilization stimulated primary production, with mixed layer integrated net primary
36 production and growth rates much higher in the fertilized areas (up to $315 \text{ mmol C m}^{-2} \text{ d}^{-1}$ and
37 up to 0.31 d^{-1} , respectively) compared to the HNLC reference site ($12 \text{ mmol C m}^{-2} \text{ d}^{-1}$ and
38 0.06 d^{-1} , respectively). Primary production was mainly sustained by nitrate uptake, with f-
39 ratios (corresponding to NO_3^- -uptake / (NO_3^- -uptake + NH_4^+ -uptake)) lying at the upper end of
40 the observations for the Southern Ocean (up to 0.9). We report high rates of nitrification (up
41 to $\sim 3 \mu\text{mol N l}^{-1} \text{ d}^{-1}$, with $\sim 90\%$ of them $< 1 \mu\text{mol N l}^{-1} \text{ d}^{-1}$) typically occurring below the
42 euphotic zone, as classically observed in the global ocean. The specificity of the studied area
43 is that at most of the stations, the euphotic layer was shallower than the mixed layer, implying
44 that nitrifiers can efficiently compete with phytoplankton for the ammonium produced by
45 remineralization at low light intensities. Nitrate produced by nitrification in the mixed layer
46 below the euphotic zone is easily supplied to the euphotic zone waters above, and nitrification
47 sustained $70 \pm 30 \%$ of the nitrate uptake in the productive area above the Kerguelen Plateau.
48 This complicates estimations of new production as potentially exportable production. We
49 conclude that high productivity in deep mixing system stimulates the N cycle by increasing
50 both assimilation and regeneration.

51

52

53

54

55

56

57 **1 Introduction**

58 The Southern Ocean is considered a High Nutrient Low Chlorophyll (HNLC) system due to a
59 combination of several factors, which include upwelling of nutrient-rich waters south of the
60 Antarctic Polar Front and a combined iron and light co-limitation of phytoplankton growth
61 (Martin, 1990; Falkowski et al., 1998; Sarmiento et al., 2004). The Southern Ocean is also
62 recognized as a major hot spot for gas exchanges and accounts for up to 20% of the global
63 ocean CO₂ uptake (Takahashi et al., 2009). Concerns regarding ongoing climate change have
64 triggered great interest in this part of the global ocean (Le Quéré et al., 2007).

65 Since the *Iron Hypothesis* formulated in the early nineties by Martin (1990) the last two
66 decades have witnessed an exponential interest by the scientific community on iron
67 availability and associated biological processes. The aim was to explore the role of iron in
68 enhancing the biological pump and the subsequent increase in the drawdown of atmospheric
69 CO₂. Numerous artificial Fe-enrichment experiments (see Boyd et al., 2007) were conducted
70 *in-situ* to explore the fertilization effect of iron (de Baar et al., 2005, 2008; Boyd et al., 2007;
71 Smetacek et al., 2012; Quéguiner, 2013). In parallel, several naturally Fe-enriched sites were
72 studied (e.g., Boyd et al., 2007) to understand the mechanisms driving such iron fertilization
73 and their impacts on biogeochemical systems without external forcing (Blain et al., 2007,
74 2008; Pollard et al., 2007, 2009; Bowie et al., 2011). The KEOPS project, carried out in the
75 Kerguelen area is dedicated to the understanding of naturally iron-fertilized system
76 functioning over a large spatial and seasonal scale. For that purpose a first cruise was
77 completed during austral summer 2005 (KEOPS1, February-March; Blain et al., 2007) and a
78 second cruise was completed during austral spring 2011 (KEOPS2, October-November,
79 2011).

80 Through its crustal interface the Kerguelen area (composed of Kerguelen Island, the
81 Kerguelen Plateau and Heard Island in the south-east) enriches the surrounding waters with
82 macronutrients and trace elements. It also strongly impacts the local oceanic physical
83 dynamics due to its Island Mass Effect (IME; Doty and Oguri, 1956). The interactions
84 between geostrophic water flow disturbances due to the presence of the island, the tidal
85 activity over the plateau, and the strong winds characterizing the area, generate internal
86 waves, eddies, jets, Ekman pumping and produces a complex hydrodynamical environment
87 (Heywood et al., 1990; Park et al., 2008; Gille et al., 2014). These characteristics are key
88 factors inducing the fertilization and the associated higher productivities around the

89 Kerguelen Island area as compared to the HNLC surrounding waters (Blain et al., 2001, 2007;
90 Fig. 1). Moreover, a third condition impacting productivity is the proximity of the Polar Front
91 (PF), which trajectory is steered by the bottom topography (Park et al., 2014). Such frontal
92 system by itself offers peculiar conditions inducing significant biological activity (de Baar et
93 al., 1995).

94 Here we report net primary production together with N-uptake (NO_3^- and NH_4^+) and
95 nitrification rates over the Kerguelen plateau and the downstream area visited during KEOPS-
96 2. Studies conducted during KEOPS1 showed a decoupling of the seasonal use of nitrate and
97 silicic acid stocks over the Kerguelen Plateau (Mosseri et al., 2008), although $\text{Si}:\text{NO}_3$
98 assimilation ratios were close to 1, in accordance with what is expected for non-limiting iron
99 conditions (Takeda, 1998; Hutchins and Bruland, 1998). Mosseri et al. (2008) attributed this
100 peculiar decoupling to the capacity of diatoms to grow on ammonium that could result from
101 high heterotrophic activity at the end of the productive season. These observations highlight
102 the potential importance of nitrogen recycling in the surface layer. In this context, the
103 objectives of the studies undertaken during KEOPS2 were:

- 104 1) to evaluate and compare the C- and N-assimilation rates during austral spring over the
105 Kerguelen Plateau, in the wake of Kerguelen Island, and at a reference HNLC site,
- 106 2) to assess the importance of recycling processes for the supply of nitrogen sources for
107 phytoplankton in the surface layer,
- 108 3) to test the intensity of nitrification and its role in the recycling of nitrogen.

109

110 **2 Materials and methods**

111 The KEOPS 2 expedition took place in the Indian sector of the Southern Ocean during early
112 spring 2011 (September to November) on board the R/V *Marion Dufresne*. Process studies
113 were conducted at 8 sites (Fig. 1), including a reference station (R-2) in a HNLC off-plateau
114 region located south-west of the Kerguelen Islands, one station (A3-2) above the Plateau, one
115 station (E4-W) on the Plateau margin, one station (F-L) north of the Polar Front to the east of
116 Kerguelen; further four stations (E-1, E-3, E4-E, E-5) in a complex recirculation system of a
117 stationary meander confined by the Polar Front.

118 At these 8 sites we performed isotope tracer experiments to assess the following rates:

119 - C-fixation rates (hereafter defined as net primary production) by spiking with ^{13}C -DIC, and
120 subsequent measurement of the ^{13}C incorporation into biomass.

121 - Ammonium and nitrate uptake rates by spiking either with $^{15}\text{N-NH}_4^+$ or $^{15}\text{N-NO}_3^-$ and
122 subsequent measurement of the ^{15}N incorporation into biomass.

123 - Nitrification rates by spiking with $^{15}\text{N-NO}_3^-$ and measuring the ^{14}N isotopic dilution of $^{15}\text{N-}$
124 nitrate resulting from the oxidation of both ammonium and nitrite by the nitrifiers. This
125 allows us to assess the second step in the nitrification process (i.e., nitrate production).

126 Surface waters were sampled at 7 to 8 depths corresponding to 75%, 45%, 25%, 16%, 4%,
127 1%, 0,3%, 0,01% of the surface photosynthetically active radiation (PAR), using Niskin
128 bottles mounted on a rosette fitted with a PAR sensor. For each light level, two acid-cleaned
129 1L polycarbonate incubation bottles were filled with seawater. The two bottles were spiked
130 with $200 \mu\text{mol L}^{-1}$ of $^{13}\text{C-HCO}_3^-$ (99 atom ^{13}C %), corresponding to a tracer addition
131 equivalent of $\approx 10\%$ of the surface seawater DIC concentration ($\approx 2\text{mM}$), and providing a
132 duplicate of net primary production. One of the bottles was spiked with $^{15}\text{N-NO}_3^-$ and the
133 other with $^{15}\text{N-NH}_4^+$ (98 atom ^{15}N %). The amount of spike added was calculated taking into
134 account the original nitrate and ammonium concentrations in order to achieve concentration
135 increments $< 10\%$. This required nutrient concentration level to be available, as obtained from
136 the analysis of preceding CTD casts. Nitrate was measured by continuous flow analysis
137 (Aminot and K rouel, 2007) and ammonium via fluorometric method (Holmes et al., 1999).
138 The continuous flow approach accuracy was assessed using reference material (Certipur,
139 Merck). The precisions were in the range of 1-4% and the limit of detection was $0.02 \mu\text{M}$ for
140 NO_3^- and NO_2^- (see also Blain et al., 2015).

141 Incubation bottles were then transferred into on-deck incubators, cooled with circulating
142 surface seawater, and wrapped in neutral density screens simulating the photometric depths.
143 Incubation experiments were stopped after 24h. This relatively long incubation time implies
144 that we probably underestimated uptake rates in case of (1) release of ^{15}N and ^{13}C to the
145 dissolved organic pool during the course of the experiment (Bronk et al., 1994; Laws et al.,
146 2002) and (2) ammonification, which would result in diluting the ^{15}N -spiked ammonium pool
147 with ^{14}N . By applying a steady state model (Glibert et al. 1982) assuming that uptake and
148 regeneration rates are equal for each nitrogen pool, which should be the case here given the
149 low and relatively constant concentration of ammonium, the factor by which ammonium
150 uptake rates are underestimated is 1.17 ± 0.23 (1 SD; minimum = 1,00; maximum = 2,36).

151 This is in the range of factors (1.5 to 2.0) suggested by Rees et al. (1995), Elskens et al.
152 (1997) and Slawyk et al. (1997). Also, there is no significant effect on the estimation of the f-
153 ratio (i.e., NO_3^- uptake/ $(\text{NO}_3^-$ uptake + NH_4^+ uptake; Dugdale and Goering, 1967), as the
154 relationship between the uncorrected and corrected f-ratio is close of 1 (0.96 ± 0.01 ; $R^2 =$
155 0.99 , p value < 0.001). Given the low underestimation, uncorrected ammonium uptake rates
156 will be presented and discussed. Moreover, we opted for long incubation times in order to
157 enhance sensitivity for detection of nitrification, and to enable the comparison with Si uptake
158 and dissolution experiments carried out over similar 24 h periods (Closset et al., 2014).

159 Both at the initial and final incubation times (initial time meaning just after spiking),
160 subsamples for nitrate (10mL) and ammonium concentrations (2 x 20mL) were directly
161 measured. A further additional 10 mL were sampled from the ^{15}N - NO_3^- incubation bottle at
162 initial and final time for assessment of initial and final ^{15}N -nitrate conditions. These
163 subsamples were filtered using 0.2 μm Acrodisc filters (Sartorius) and stored at -20°C , for
164 later analysis of nitrate isotopic composition. The remaining seawater was filtered on pre-
165 combusted (450°C) glass fiber filters (Sartorius, MGF, nominal porosity 0.7 μm , 25 mm
166 diameter). Filters were placed in pre-combusted scintillation vials, dried at 50°C and stored in
167 the dark at room temperature until further analysis at the home based laboratory.

168 Particulate organic nitrogen (PON) and particulate organic carbon (POC) concentrations
169 along with their ^{15}N and ^{13}C abundances (atom ^{13}C and ^{15}N %) were analysed via an
170 elemental analyser-isotope ratio mass spectrometer (EA-IRMS) using the method described in
171 Savoye et al. (2004).

172 Atom ^{15}N % for nitrate at initial and final time was measured using the denitrifier method
173 (Sigman et al., 2001). Briefly, 20-30 nmol of nitrate were quantitatively converted to N_2O gas
174 by denitrifying bacteria (*Pseudomonas aureofaciens*) that lack an active N_2O reductase. The
175 ^{15}N abundance of the N_2O was measured by gas chromatography/isotope ratio mass
176 spectrometry (GC/IRMS) with on-line cryo-trapping.

177 C-assimilation and ammonium uptake rates (ρNH_4^+) were calculated from the equations of
178 Dugdale and Goering (1967) where Atom% $^{13}\text{C}_{\text{DIC}}$ ti and Atom% $^{15}\text{NH}_4^+$ ti were calculated
179 and the other parameters were measured. For C-fixation this equation writes:

180

$$V = \frac{(\text{atom}\% \text{ } ^{13}\text{C}_{\text{POC}_{\text{tf}}})}{\text{time} \cdot (\text{atom}\% \text{ } ^{13}\text{C}_{\text{DIC}_{\text{ti}}})} \quad (1)$$

181
$$NPP = [POC_{tf}] \cdot V \quad (2)$$

182 Where V is the specific C assimilation rate (in d⁻¹), NPP net primary production (in μmol C l⁻¹
 183 d⁻¹), atom % ¹³C the measured abundances minus the natural abundances, and tf & ti refer to
 184 the final and initial time of incubation, respectively. Except for nitrate for which initial
 185 abundances were measured, the initial abundances for both DIC and NH₄⁺ were calculated by
 186 taking into account the spike addition and isotopic abundance.

187 The nitrate uptake rate (ρNO₃⁻) was first corrected for the isotope dilution effect during
 188 incubation and then assessed with the following equations (Nelson and Goering, 1977a, b):

189
$$V NO_3^- = \frac{atom \% ^{15}N_{PON_{tf}}}{time \cdot \sqrt{atom \% ^{15}NO_{3ti}^- \cdot atom \% ^{15}NO_{3tf}^-}} \quad (3)$$

190

191
$$\rho NO_3^- = [PON_{tf}] \cdot V NO_3^- \quad (4)$$

192

193 The nitrification (RNO₃⁻) rate was assessed using the integrated rate equation of the
 194 Blackburn model (Blackburn, 1979; Elskens et al. 2005):

195

196
$$RNO_3^- = \frac{\ln \left(atom \% ^{15}NO_{3ti}^- / atom \% ^{15}NO_{3tf}^- \right) \cdot [NO_{3tf}^- - NO_{3ti}^-]}{time \cdot \left([NO_{3tf}^-] \sqrt{[NO_{3ti}^-]} \right)} \quad (5)$$

197

198 The uncertainty on uptake (NPP, ρNH₄ and ρNO₃) and nitrification (RNO₃) rates were
 199 assessed using Monte-Carlo simulations assuming normal distributions for all variables.

200 The modelled nitrification rates were screened for consistency between observed evolutions
 201 of nitrate concentrations over the duration of the incubation experiment and measured nitrate
 202 uptake rates. The difference between nitrate uptake and nitrification should be compatible
 203 with the change in nitrate concentration over the duration of the incubation experiment, taking
 204 into account a 10% precision (relative standard deviation SD) on rates and concentrations
 205 measurements. When the rates given by the model were incompatible with temporal evolution
 206 of nitrate concentration, nitrification experiments were considered as being flawed and were

207 left out of the dataset. We point out that measuring nitrification rates under conditions of high
208 ambient nitrate is methodologically challenging. Indeed, because ambient nitrate is high
209 sensitivity is poor. The latter is estimated at $0.26 \mu\text{mol l}^{-1} \text{d}^{-1}$ considering how much
210 nitrification is needed to change the isotopic composition of the nitrate pool by 2 SD.
211 Furthermore, the measurement precision ($\pm 0.26 \mu\text{mol l}^{-1} \text{d}^{-1}$; estimated by taking into account
212 the precision on the isotopic measurement; 2 SD) is poor. We note that such values for
213 sensitivity and precision of nitrification rates analysis exceed most of the nitrification rates
214 reported to date for the open ocean (Ward, 2008).

215

216 **3 Results**

217 Except for station (F-L) north of the Polar Front, the different water masses and associated
218 biogeochemical properties were characteristic of the Antarctic Zone: relatively warmer waters
219 in the upper mixed layer (defined following the density criterion of 0.02 kg m^{-3} ; de Boyer
220 Montégut et al., 2004) and the remnants of winter water in the lower part of the mixed layer
221 (temperature minimum layer; Park et al., 2008). South of the Polar Front, mixed layer macro-
222 nutrient levels were high and their distributions were relatively uniform between stations
223 (Blain et al., 2015; Closset et al., 2014), with an average nitrate concentration of $\sim 25 \mu\text{mol l}^{-1}$
224 (Fig. 2a). In agreement with a scenario of progressive nutrient consumption during meridional
225 water transfer northward across the Antarctic Circumpolar Current (Sigman et al., 1999;
226 Sarmiento et al., 2004), the station north of the Polar Front (F-L) had higher surface
227 temperatures (1 to 2°C – data not shown) and lower nitrate concentrations (Fig. 2a). Both
228 ammonium and nitrite concentrations in the mixed layer were low and remained relatively
229 constant over time ($\sim 0.25 \mu\text{mol l}^{-1}$), indicating a tight balance between production and
230 consumption processes (Fig. 2b, c and Annex). There is, however, an exception for station F-
231 L north of the Polar Front where a gradient in ammonium concentration was observed within
232 the mixed layer. This contrasts most stations where an ammonium accumulation (up to 0.5
233 $\mu\text{mol l}^{-1}$) was observed below the mixed layer (Fig. 2b). An ammonium accumulation
234 probably results from an imbalance between ammonium production (remineralization) and
235 consumption processes (assimilation + nitrification) (Blain et al., 2015).

236 Both particulate organic C and N concentrations (POC and PON) increased from the HNLC
237 reference station (R-2) to the meander stations (E stations), and then to the high productive
238 sites, over the Kerguelen Southeast Plateau (A3-2) and at the margin (E4-W) as well as

239 further north of the Polar Front (F-L) (Fig. 3). Overall, this spatial distribution of
240 phytoplankton biomass is in agreement with satellite chl-a observations (Fig. 1). A positive
241 relationship is apparent between biomass ($\mu\text{mol l}^{-1}$) and assimilation rates ($\mu\text{mol l}^{-1} \text{d}^{-1}$), as
242 well as specific uptake rate ($V; \text{d}^{-1}$; growth rate) both for carbon and nitrogen (Fig. 3a, b, c, d).
243 Therefore a negative relationship holds between biomass and doubling time ($T_d = \ln(2)/V$; in
244 days) (Fig. 3e, f). The bloom over the Kerguelen Plateau (A3-2 and E4-W) and north of the
245 Polar Front (F-L) presented higher assimilation rates per unit of C and N biomass than the
246 stations in the HNLC area (R-2) and the meander (E stations).

247 In general, vertical profiles of net primary production followed light availability in the mixed
248 layer, with a sharp decrease below the euphotic layer depth (Zeu; 1% surface PAR depth)
249 (Fig. 4). Primary production extended well below Zeu, although at much lower rates than at
250 shallower depths. This was particularly obvious for the most productive stations; primary
251 production rates were still 0.36, 0.37, and 0.12 $\mu\text{mol C l}^{-1} \text{d}^{-1}$ at the 0.3% PAR level, as
252 compared to rates of 11.9, 8.3, and 6.2 $\mu\text{mol C l}^{-1} \text{d}^{-1}$ in the near-surface; for stations F-L, E4-
253 W, and A3-2, respectively. At the 0.01% PAR level we observed still significant primary
254 production at F-L, E4-W and A3-2 stations (0.12, 0.06 and 0.08 $\mu\text{mol C l}^{-1} \text{d}^{-1}$, respectively),
255 while at the least productive sites primary production at 0.01% PAR was low to non
256 detectable (Fig. 4).

257 Vertical profiles of NO_3^- assimilation rates closely paralleled the vertical evolution of primary
258 production (Fig. 4) but the decrease in NH_4^+ assimilation with depth was less severe than that
259 for NO_3^- . Nitrate was still preferentially assimilated over ammonium at most of the stations,
260 except at the HNLC reference station (Fig. 5a). This resulted in high f-ratios *i.e.* NO_3^-
261 uptake/ $(\text{NO}_3^-$ uptake + NH_4^+ uptake) (Dugdale and Goering, 1967) which increased in the
262 euphotic layer from ~0.4 at the less productive HNLC reference station to ~0.9 at station F-L,
263 north of the Polar Front.

264 We observe significant nitrification rates in the mixed layer with maximal rates generally near
265 the bottom of the euphotic layer (Fig; 4 and 5b). Nitrification reached up to ~ 3 $\mu\text{mol N l}^{-1} \text{d}^{-1}$,
266 though ~90% of the values were < 1 $\mu\text{mol N l}^{-1} \text{d}^{-1}$ (Fig. 4).

267

269 **4.1 High primary production in naturally iron-fertilized blooms**

270 Several massive blooms occur in the core of the Antarctic Circumpolar Current in the
271 Kerguelen area (Fig. 1): (i) over the Kerguelen Southeast Plateau, remarkably constrained by
272 the bathymetry, (ii) in a plume extending eastward through the interaction between the Polar
273 Front jet, crossing the plateau in a narrow mid-depth channel just to the south of the
274 Kerguelen Island, and the rise bordering the basin to the north, (iii) and to the easternmost
275 part of the study area in a zone of retroflexion of the Polar Front and of eddy mixing between
276 Antarctic and Sub–Antarctic Surface Waters (see Park et al., 2014). This complex distribution
277 is in agreement with an input of iron from the interaction between the iron-deficient Antarctic
278 Circumpolar Current and the local bathymetry (Blain et al., 2007; Sokolov and Rintoul,
279 2007). Trace metals, and iron in particular, are required for many important cellular processes
280 such as photosynthesis (including photo–adaptation), respiration, and nitrate reduction. Iron-
281 enrichment experiments ranging from bottle incubations to large scale open-ocean
282 amendment studies have demonstrated that iron supply stimulates phytoplankton growth in
283 the Southern Ocean (Martin, 1990; de Baar et al., 1990, 2005; Boyd et al., 2007). Primary
284 production up to $130 \text{ mmol C m}^{-2} \text{ d}^{-1}$ has been reported in these iron-fertilized patches (Gall et
285 al., 2001; Gervais et al., 2002; Coale et al., 2004; Smetacek et al., 2012). Naturally iron
286 fertilized systems usually present higher rates of primary production: e.g., up to $\sim 275 \text{ mmol C}$
287 $\text{m}^{-2} \text{ d}^{-1}$ over the South Georgia plateau (Korb et al., 2005); and up to $\sim 250 \text{ mmol C m}^{-2} \text{ d}^{-1}$
288 within the fast-flowing, iron-rich jet of the Polar Front in the Atlantic sector (Jochem et al.,
289 1995) and in the iron–fertilized plume of Crozet Islands (Seeyave et al., 2007). The
290 production rates reported here for the fertilized areas (35 to $315 \text{ mmol C m}^{-2} \text{ d}^{-1}$) are in line
291 with these previous studies (Table 1), confirming that the spring phytoplankton blooms
292 developing over, and downstream of the Kerguelen Plateau are sustained by very high rates of
293 net primary production. Primary production in the adjacent HNLC area (R-2; $\sim 13 \text{ mmol C m}^{-2}$
294 d^{-1}) is lower and in agreement with the primary production reported for the HNLC pelagic
295 zone in the Southern Ocean (from 4 to $33 \text{ mmol C m}^{-2} \text{ d}^{-1}$; Arrigo et al., 2008).

296 At the most productive stations of the different bloom sites, primary production is still
297 occurring below 1% PAR attenuation, which is generally considered to represent the lower
298 limit of the euphotic layer. Such an observation is not unusual and this has been recently

299 discussed by Marra et al. (2014). In the present study primary production rates generally reach
300 zero within the confinement of the mixed layer, fluxes were therefore integrated between
301 surface and bottom of the mixed layer. Moreover, the mixed layer is characterized by a steep
302 density gradient at the bottom, implying uniform biogeochemical properties and limited
303 exchanges with the underlying ocean. Primary production, therefore, affects and is affected by
304 the biogeochemical properties of this layer. Note however than at stations E-3 and E-5 the
305 euphotic layer extends deeper than the mixed layer, and accordingly there was still some
306 primary production measurable below the mixed layer. Therefore, for these two stations,
307 integration of primary production over the mixed layer underestimates primary production
308 integrated over the euphotic layer by 40 and 20%, respectively.

309 Notwithstanding the complex interplay between biogeochemical and physical processes in
310 this large-scale natural iron-fertilization experiment, we do observe a strong, relatively simple
311 linear relationship between the amount of biomass ($\mu\text{mol C L}^{-1}$ and $\mu\text{mol N L}^{-1}$), and both,
312 assimilation rates ($\mu\text{mol C L}^{-1} \text{d}^{-1}$ and $\mu\text{mol N L}^{-1} \text{d}^{-1}$) and specific growth rates (d^{-1}) (Fig. 3).
313 The increase in biomass normalized primary production with increasing biomass cannot be
314 explained by variations in macro-nutrient concentrations or temperature in the mixed layer.
315 Indeed, the maximum difference in temperature was less than 2°C and according to the
316 growth-temperature relationship described in Eppley (1972) such a small range of
317 temperature cannot explain the large change in growth rate. Throughout the study period the
318 uniformly high macro-nutrient concentrations (Blain et al., 2015; Closset et al., 2014; Fig. 2)
319 remained at levels preventing any Si, P or N limitation of phytoplankton growth (e.g., Sarthou
320 et al., 2005, and reference therein).

321 The likeliness of a larger supply of iron and trace metals over the Kerguelen Plateau and north
322 of the Polar Front (Martin, 1990; de Baar et al., 2005; Boyd et al., 2007; Blain et al., 2007)
323 stands out as the most important cause for the observed differences in primary production
324 (from ~ 0 to $9 \mu\text{mol C l}^{-1} \text{d}^{-1}$) and C growth rate (from <0.1 and 0.3d^{-1}) between stations (Fig.
325 3). Over the shallow plateau iron is supplied through the interaction of the bottom waters with
326 sediments and possible igneous outcrops. By this process, subsurface water is becoming
327 enriched in iron, which subsequently can be efficiently supplied to the mixed layer via
328 vertical mixing (Blain et al., 2007; Park et al., 2008). At the Polar Front iron fertilization
329 results from the previously described enrichment over the plateau and the spreading of this
330 enrichment eastward through the additional interaction between the Polar Front jet and local

331 bathymetry (Mongin et al., 2008; Sanial et al., 2015). This mode of supply can be compared
332 with the Polar Front associated bloom in the Atlantic sector, where iron is supplied by lateral
333 advection from the Patagonian shelves and islands in the Scotia Ridge area (de Baar et al.,
334 1995; Löscher et al., 1997) or by direct lithogenic aerosol deposition (Quéguiner et al., 1997).
335 Similar increases in growth rate driven by the degree of iron fertilization (Fig. 3) were
336 reported earlier for the Southern Ocean (e.g., the growth rate increase from <0.1 to 0.5 d^{-1} in
337 the SOIREE fertilized patch; Gall et al., 2001).

338 Net primary production during summer over the Kerguelen Plateau (January-February,
339 KEOPS 1; Mosseri et al., 2008; Lefèvre et al., 2008), reached values close to $\sim 80 \text{ mmol C m}^{-2}$
340 d^{-1} . Such rates are lower than those for spring presented here ($\sim 200 \text{ mmol C m}^{-2} \text{ d}^{-1}$) (Table 1).
341 This seasonal pattern is in agreement with satellite chl-a distribution data showing that the
342 bloom starts in early November, reaches its maximum level in late November-early
343 December, and collapses in January-February (Mongin et al., 2008). Contrasting with the
344 spring situation studied here (KEOPS 2) the summer situation (KEOPS 1) does not show any
345 relationship between biomass and primary production or growth rate (Fig. 6). In early
346 February (KEOPS 1), primary production and growth rate rapidly decreased in the euphotic
347 layer from about 14 down to $2 \mu\text{mol C l}^{-1} \text{ d}^{-1}$, and from ~ 0.3 down to 0.01 d^{-1} , respectively.
348 Associated with these changes, the mixed layer production system evolved from being
349 autotrophic, characteristic for spring, to heterotrophic with respiration exceeding
350 photosynthesis (Lefèvre et al., 2008; Christaki et al., 2014). With nitrate and phosphate at
351 non-limiting concentrations, a top-down control of phytoplankton development (mostly
352 diatoms; George et al., 2014; Sackett et al., 2014) is the most likely cause of this change
353 during the decay of the bloom in late summer (KEOPS 1; Carlotti et al., 2008; Brussaard et
354 al., 2008; Sarthou et al., 2008). A Si limitation of diatom growth during this period cannot be
355 ruled out either, since measured silicic acid concentrations ($\sim 1 \mu\text{mol l}^{-1}$) are significantly
356 below measured half saturation constants for Si-uptake ($5\text{-}15 \mu\text{mol l}^{-1}$; Mosseri et al., 2008).
357 However, Fv/Fm ratios (ratio of variable fluorescence Fv to the maximum fluorescence Fm,
358 quantitatively related to the efficiency of photochemistry – Falkowski and Raven, 1997) over
359 the plateau in late summer remained high, indicating that the phytoplankton community was
360 relieved from nutrient stress, including iron stress (Timmermans et al., 2008).

361 To conclude, the resulting increase in integrated primary production (up to 8 times; Table 1)
362 between fertilized (Plateau and Polar Front) and unfertilized areas (HNLC reference site) is

363 similar to the largest increase reported for artificial iron addition experiments worldwide
364 (Boyd et al., 2007; up to 10 times). Despite the much higher primary production for the
365 fertilized area in comparison with the HNLC area, the export of organic matter remains
366 relatively small during spring and summer (Savoie et al., 2008; Planchon et al., 2015). Low
367 export efficiency suggests that the products of primary production are mainly recycled within
368 the mixed layer by an efficient microbial loop (Sarhou et al., 2008; Obernosterer et al., 2008;
369 Christaki et al., 2014; Malits et al., 2014). The carbon sequestration efficiency induced by
370 iron-fertilization remains proportionally relatively low (Jacquet et al., 2008, 2015).

371 **4.2 Upper Ocean N cycling: high f-ratios and nitrification rates in deep** 372 **productive mixed layer**

373 Integrated N-uptake rates and f-ratios lie in the upper range of values reported for the
374 Southern Ocean (Table 1), and are indicative of a nearly completely NO_3^- -based primary
375 production (Sambrotto and Mace, 2000; Savoie et al., 2004; Mulholland and Lomas, 2008;
376 Cochlan, 2008). The f-ratio increases with measured N-uptake rates ($\text{NO}_3^- + \text{NH}_4^+$), from ~ 0.3
377 in the less productive HNLC reference station to ~ 0.8 in the productive areas over the
378 Kerguelen Plateau and north of the Polar Front (Fig. 5a; Table 1). Such relationship with
379 productivity is in agreement with an enhancement of both specific and absolute NO_3^- uptake
380 rates under iron-replete conditions (Van Leeuwe et al., 1997; Timmermans et al., 1998;
381 Franck et al., 2000; Cochlan et al., 2002; Coale et al., 2004; Lucas et al., 2007) (Fig. 3), as
382 well as with the natural variability of the f-ratio in the Southern Ocean related to productivity
383 (HNLC vs. productive areas; Cochlan, 2008). Below the euphotic layer, ammonium is
384 preferentially assimilated over nitrate, with f-ratios ranging between 0.1 and 0.5 (data not
385 shown). Assimilation of nitrate is energetically more demanding than assimilation of
386 ammonium and should be more dependent on light. Once nitrate has been transported into the
387 cell, it has to be further reduced into ammonium before it can be assimilated (Mulholland and
388 Lomas, 2008). At the end of summer, the f-ratio over the plateau decreases rapidly, from 0.6
389 to 0.2, indicating that the system evolved from a nitrate-based to an ammonium-based
390 primary production (Mosseri et al., 2008; P. Raimbault, KEOPS 1 database). Such an
391 evolution is in agreement with an increase in ammonium availability in a decaying bloom
392 (Sambrotto and Mace, 2000; Cochlan, 2008). Note that our f-ratios are most probably
393 overestimated because they do not take into account the assimilation of dissolved organic
394 nitrogen by phytoplankton (Bronk et al., 2007). However, we note that urea uptake, a proxy

395 for dissolved organic N assimilation, is usually relatively low south of the Polar Front, where
396 dissolved inorganic N is abundant (Waldron et al., 1995; Sambrotto and Mace, 2000; Savoye
397 et al., 2004).

398 Nitrification rates are high (up to $3 \mu\text{mol l}^{-1} \text{d}^{-1}$, with ~90% of the cases $<1 \mu\text{mol l}^{-1} \text{d}^{-1}$) at low
399 light intensities, and insignificant (below our detection limit) at high light intensities (Figs. 4
400 and 5b). Such rates (~90% of the cases) are in the range of maximum rates reported for the
401 open ocean (up to $0.75 \mu\text{mol l}^{-1} \text{d}^{-1}$) in the Peru Upwelling (Lipschultz et al., 1991; Ward,
402 2008), and above the one reported for the Southern Ocean ($<0.1 \mu\text{mol l}^{-1} \text{d}^{-1}$; Olson, 1981;
403 Bianchi et al., 1997). The Southern Ocean nitrification data available in the literature pertain
404 to fall and winter, seasons during which primary production and remineralization are expected
405 to be low. Nitrification occurs in two steps, the oxidation of ammonium to nitrite and the
406 oxidation of nitrite to nitrate, mediated by distinct groups of microorganisms (Ward, 2008).
407 We only assessed the second step of the nitrification processes (i.e., nitrate production).
408 However, a balance between the first and second steps is likely, given the relatively low and
409 constant ammonium and nitrite concentrations in the mixed layer (Fig. 2) even at the seasonal
410 scale (Fripiat et al., in revision).

411 The observed variation of nitrification with depth supports the fact that the process is partly
412 light-inhibited (Fig. 5b) and this is in agreement with what we know about the distribution of
413 nitrification in the ocean (Hagopian and Riley, 1998; Ward, 2008). High nitrification rates are
414 usually reported near the bottom of the euphotic layer where organic matter is still abundant
415 and light is much reduced, allowing the nitrifiers to compete with phytoplankton for the
416 ammonium produced by remineralization (Lipschultz et al., 1991; Ward, 2008). Below the
417 euphotic layer, organic matter degradation and organic matter export lead to ammonium
418 release which is *in fine* nearly-quantitatively converted into nitrate (Ward and Zafiriou, 1988;
419 Newel et al., 2011). As the process closing the internal N cycle ($\text{NO}_3^- \rightarrow \text{PON} \rightarrow \text{NO}_3^-$)
420 nitrification likely tracks primary production. The unusual high rates of nitrification across the
421 study area likely result from the particularly high rates of primary production, which are in the
422 upper range for those observed in the Southern Ocean (section 4.1).

423 The particularity of our study is that a significant fraction of the mixed layer (except for
424 stations E-3 and E-5) extends below the euphotic layer (Fig. 4). The nitrate produced by
425 nitrification at low-light intensities can be easily transported into the euphotic layer and
426 supports directly regenerated primary production. Such findings have profound consequences

427 on the concept of new production (Dugdale and Goering, 1967; Eppley and Petterson, 1979).
428 Under steady-state conditions and averaged over appropriate time scales, new production is
429 the fraction of primary production that can be exported from the euphotic layer, without
430 depleting the system in nutrients. New production is therefore balanced by the supply of new
431 nutrients into the euphotic layer. New nutrients are distantly produced, supplied into the
432 euphotic layer by water mixing or atmospheric deposition/exchange, and assimilated during
433 the vegetative season. Generally in the ocean, the euphotic layer is deeper than the mixed
434 layer (e.g., in the low-latitude oceans). Under such conditions, nitrate produced by
435 nitrification below the euphotic layer can only become available for subsequent primary
436 production by diapycnal mixing, through the lower boundary of the mixed layer. In this
437 context, nitrate has generally been considered as a new nutrient (Dugdale and Goring, 1967),
438 especially in the Southern Ocean where it is also considered as the dominant nitrogen source
439 assuming negligible N₂ fixation. Following this rationale, new production in the Southern
440 Ocean is usually calculated by multiplying the primary production with the f-ratio (Eppley
441 and Peterson, 1979; Savoye et al., 2004). However, nitrification in a deep mixed layer may
442 fuel an important input of nitrate in the euphotic layer with, therefore, a significant fraction of
443 nitrate-based primary production being actually regenerated production. To calculate correctly
444 the new production (f-ratio x NPP), one needs to subtract the nitrification term from the
445 nitrate uptake term (Yool et al., 2007). The nitrification depth profiles were well resolved at
446 only 5 stations, permitting nitrification rates to be integrated over the mixed layer depth
447 (Table 1). For the productive stations A3-2 and E4-W where low-light (< 1% PAR) prevails
448 over 40-70% of the mixed layer, nitrification decreased the f-ratio from $\sim 0.8 \pm 0.0$ to $\sim 0.2 \pm$
449 0.2 , implying that 70 ± 30 % of the nitrate uptake was sustained by nitrification. This is in
450 agreement with Fripiat et al. (in revision) who simulated the change of the fixed N pools and
451 their isotopic composition ($\delta^{15}\text{N}$ and $\delta^{18}\text{O}$) from October to February for the Kerguelen
452 Plateau and show that nitrification can account for 40 to 80% of the seasonal nitrate
453 assimilation. The significance of nitrification above the plateau was also inferred from the
454 temporal change of the nitrate isotopic composition during spring (KEOPS 2), sustaining ~ 50
455 % of the nitrate assimilation (Dehairs et al., 2015). By inspecting the short-term changes in
456 the meander area, the contribution of nitrification to nitrate assimilation varies significantly
457 between successive visits. During the first visit in the meander area (E-1), integrated
458 nitrification was higher than that of integrated nitrate uptake. This implies that 100% of the
459 nitrate assimilated by phytoplankton originates from regeneration. This contribution decreases

460 during the two subsequent visits implying the f-ratio to change from 0.7 to 0.3 and from 0.7 to
461 0.6 for E4-E and E-5, respectively. The low contribution of nitrification during the last visit is
462 in agreement with a mixed layer depth (MLD) being shallower than the euphotic layer depth,
463 and implying a vertical segregation between nitrate uptake and nitrification delimited by a
464 sharp density gradient defining the MLD.

465 High mixed layer nitrification rates in the fertilized area are also in agreement with (i) the
466 measured low carbon export efficiency ($\text{NPP}/^{234}\text{Th-export}$, with $^{234}\text{Th-export}$ estimated at
467 100m; Planchon et al., 2014), and (ii) the low seasonal nitrate depletion (Mosseri et al., 2008)
468 despite high nitrate assimilation rates in the mixed layer. Significant nitrification can also
469 explain why silicic acid is depleted (with high biogenic silica production/dissolution ratio) but
470 not nitrate (Mosseri et al., 2008; Closset et al., 2014). Si:NO₃ assimilation ratios were close to
471 1 (Mosseri et al., 2008; Closset et al., 2014), in accordance with what is expected for non-
472 limiting iron conditions (Takeda, 1998; Hutchins and Bruland, 1998). Without nitrification,
473 nitrate should be depleted similar to silicic acid. The hypothesis put forward by Mosseri et al.
474 (2008), attributes this peculiar decoupling to the capacity of diatoms to grow on ammonium
475 resulting from high heterotrophic activity. Such a hypothesis appears unlikely here since for
476 all stations, except R-2, ammonium assimilation rates are much lower than nitrate assimilation
477 rates. Thus, we hypothesize that in a deep mixing system nitrifiers can efficiently compete
478 with phytoplankton for ammonium.

479

480 **5 Conclusions**

481 This study confirms the impact of iron-fertilization on primary production in the Southern
482 Ocean. Naturally fertilized areas sustain a much higher integrated primary production (up to
483 $315 \text{ mmol C m}^{-2} \text{ d}^{-1}$) and growth rates (up to 0.31 d^{-1}) than unfertilized HNLC areas (12 mmol
484 $\text{C m}^{-2} \text{ d}^{-1}$; 0.06 d^{-1} , respectively). Primary production in the euphotic layer of the fertilized
485 areas is mainly sustained by nitrate uptake (f-ratio up to 0.9). In the unfertilized areas, the
486 contribution of ammonium to primary production increases. However, part of the nitrate
487 assimilation by phytoplankton is provided from mixed layer nitrification which is high (up to
488 $\sim 3 \mu\text{mol N l}^{-1} \text{ d}^{-1}$, with $\sim 90\%$ of them $< 1 \mu\text{mol N l}^{-1} \text{ d}^{-1}$) and presents maximum rates at the
489 base of the euphotic zone and below. Such high nitrification rates can be explained by (i) a
490 deep mixed layer -encompassing the euphotic layer- allowing nitrate assimilation and
491 regeneration to take place within the same water mass and (ii) the especially high rates of

492 primary production making the studied Kerguelen area one of the most productive systems in
493 the open ocean, likely stimulating nitrogen N assimilation and regeneration. All these
494 conditions likely contribute to creating a favorable environment for nitrifiers.

495

496

497

498 **Acknowledgements**

499 Our warm thanks go to the Captain, officers and crew of the R/V *Marion Dufresne* for their
500 support during the KEOPS 2 field work. This research was supported by the Federal Belgian
501 Science Policy Office (BELSPO), Science for Sustainable Development (SSD) program
502 (contract SD/CA/05A); Flanders Research Foundation (FWO grant G071512N); VUB
503 Strategic Research Plan. François Fripiat is a post-doctoral fellow with the Flanders Research
504 Foundation (FWO, Belgium). Camila Fernandez was partially funded by Fondap 15110027.
505 Lennin Florez-Leiva received support from the LIA MORFUN project. The KEOPS 2 project
506 was supported by the French Research program of INSU-CNRS LEFE-CYBER ('Les
507 enveloppes fluides et l'environnement' – 'Cycles biogéochimiques, environnement et
508 ressources'), the French ANR ('Agence Nationale de la Recherche', SIMI-6 program), the
509 French CNES ('Centre National d'Etudes Spatiales') and the French Polar Institute IPEV
510 (Institut Polaire Paul-Emile Victor). The altimeter and colour / temperature products for the
511 Kerguelen area were produced by Ssalto/Duacs and CLS with support from CNES.

512

513 **References**

- 514 Aminot, A., and K erouel, R.: Dosage automatique des nutriments dans les eaux marines:
515 methods en flux continu, Ed. Ifremer, 2007.
- 516 Arrigo, K.R., van Dijken, G.L. and Bushinsky, S.: Primary production in the Southern Ocean,
517 1997-2006, *Journal of Geophysical Research* 113, C08004, doi:10.1029/2007JC004551,
518 2008.
- 519 Bianchi, M., Feliatra, F., Tr guer, P., Vincedeau, M.-A . and Morvan, J. : Nitrification rates,
520 ammonium and nitrate distribution in upper layers of the water column and in sediments of
521 the Indian sector of the Southern Ocean, *Deep-Sea Research Part II*, 44, 1017-1032, 1997.
- 522 Blackburn, T.H.: A method for measuring rates of NH_4^+ turnover in anoxic marine sediments
523 using a $^{15}\text{N-NH}_4^+$ dilution technique, *Application for Environmental Microbiology*, 37, 760-
524 765.
- 525 Blain, S., Capparos, J., Gu neugu s, A., Obernosterer, I. and Oriol, L.: Distributions and
526 stoichiometry of dissolved nitrogen and phosphorus in the iron fertilized region near
527 Kerguelen (Southern Ocean), *Biogeosciences*, 12, 623-635, 2015.
- 528 Blain, S., Qu guiner, B., and Trull, T.W.: The natural iron fertilization experiment KEOPS
529 (KErguelen Ocean and Plateau compared Study): an overview, *Deep-Sea Research Part II*, 55,
530 559-565, 2008.
- 531 Blain, S., Qu guiner, B, Armand, L., Belviso, S., Bombled, B., Bopp, L., Bowie, A., Brunet,
532 C., Brussaard, C., Carlotti, F., Christaki, U., Corbi re, A., Durand, I., Ebersbach, F., Fuda, J.-
533 L., Garcia, N., Gerringa, L., Griffiths, B., Guigue, C., Guillerm, C., Jacquet, S., Jeandel, C.,
534 Laan, P., Lef vre, D., Lo Monaco, C., Malits, A., Mosseri, J., Obernosterer, I., Park, Y.-H.,
535 Picheral, M., Pondaven, P., Remenyi, T., Sandroni, V., Sarthou, G., Savoye, N., Scouarnec,
536 L., Souhaut, M., Thuiller, D., Timmermans, K., Trull, T., Uitz, J., van Beek, P., Veldhuis, M.,
537 Vincent, D., Viollier, E., Vong, L. and Wagener, T.: Effect of natural iron fertilization on
538 carbon sequestration in the Southern Ocean, *Nature*, 446, 1070-1074,
539 doi:10.1038/nature05700, 2007.
- 540 Blain, S., Tr guer, P., Belviso, S., Bucciarelli, E., Denis, M., Desabre, S., Fiala, M., Jezequel,
541 V.M., Lefevre, J., Mayzaud, M., Marty, J.-C and Razouls, S.: A biogeochemical study of the

542 island mass effect in the context of the iron hypothesis : Kerguelen Islands, Southern Ocean.
543 Deep-Sea Research Part I, 48, 163-187., 2001.

544 Bowie, A., Trull, T.W. and Dehairs, F.: Estimating the sensitivity of the subantarctic zone to
545 environmental change: the SAZ-Sense project, Deep-Sea Research Part II, 58(21-22), 2051-
546 2058, 2011.

547 Boyd, P.W., Jickells, T., Law, C.S., Blain, S., Boyle, E.A., Buesseler, K.O., Coale, K.H.,
548 Cullen, J.J., de Baar, H.J.W., Follows, M., Harvey, M., Lancelot, C., Levasseur, M., Owens,
549 N.P.J., Pollard, R., Rivkin, R.B., Sarmiento, J., Schoemann, V., Smetacek, V., Takeda, S.,
550 Tsuda, A., Turner, S. and Watson, A.J.: Mesoscale Iron Enrichment Experiments 1993-2005:
551 Synthesis and future directions, Science, 315, 612, doi:10.1126/science.1131669, 2007.

552 Bronk, D.A., See, J.H., Bradley, P. and Killberg, L.: DON as a source of bioavailable nitrogen
553 for phytoplankton. Biogeosciences, 4, 283-296, 2007.

554 Bronk, D.A., Glibert, P.M. and Ward, B.B.: Nitrogen uptake, dissolved organic nitrogen
555 release, and new production, Science, 265, 1843-1846, 1994.

556 Brussaard, C.P.D., Timmermans, K.R., Uitz, J. and Veldhuis, M.J.W.: Virioplankton
557 dynamics and virally induce phytoplankton lysis versus microzooplankton grazing southeast
558 of the Kerguelen (Southern Ocean), Deep-Sea Research Part II, 55, 752-765, 2008.

559 Carlotti, F., Thibault-Botha, D., Nowaczyk, A. and Lefèvre, D.: Zooplankton community
560 structure, biomass and role in carbon fluxes during the second half of a phytoplankton bloom
561 in the eastern sector of the Kerguelen shelf (January-February 2005), Deep-Sea Research Part
562 II, 55, 720-733, 2008.

563 Christaki, U., Lefèvre, D., Georges, C., Colombet, J., Catala, P., Courties, C., Sime-Ngando,
564 T., Blain, S., and Obernosterer, I.: Microbial food web dynamics during spring phytoplankton
565 blooms in the naturally iron-fertilized Kerguelen area (Southern Ocean). Biogeosciences, 11,
566 6739-6753, 2014.

567 Closset I., Lasbleiz, M., Leblanc, K., Quéguiner, B., Cavagna, A.-J., Elskens, M., Navez, J.
568 and Cardinal, D.: Seasonal evolution of net and regenerated silica production around a natural
569 Fe-fertilized area in the Southern Ocean estimated from Si isotopic approaches,
570 Biogeosciences, 11, 1-20, doi.10.5194/bg-11-1-2014, 2014.

571 Cochlan, W.P.: Nitrogen Uptake in the Southern Ocean. *In: Nitrogen in the Marine*
572 *Environment*, 2nd Edition, D.G. Capone, D.A. Bronk, M.R. Mulholland, and E.J. Carpenter
573 [Eds.]. Academic Press, Elsevier, pp. 569-596, 2008.

574 Cochlan, W.P., D.A. Bronk, and Coale, K.H.: Trace metals and nitrogenous nutrition of
575 Antarctic phytoplankton: experimental observations in the Ross Sea. *Deep-Sea Res. II* 49:
576 3365-3390, 2002.

577 Coale, K.H., Johnson, K.S., Chavez, F.P., Buesseler, K.O., Barber, R.T., Brzezinski, M.A.,
578 Cochlan, W.P., Millero, F.J., Falkowski, P.G., Bauer, J.E., Wanninkhof, R.H., Kudela, R.M.,
579 Altabet, M.A., Hales, B.E., Takahashi, T., Landry, M.R., Bidigare, R.R., Wang, X., Chase, Z.,
580 Strutton, P.G., Friederich, G.E., Gorbunov, M.Y., Lance, V.P., Hilting, A.K., Hiscock, M.R.,
581 Demarest, M., Hiscock, W.T., Sullian, K.F., Tanner, S.J., Gordon, R.M., Hunter, C.N., Elrod,
582 V.A., Titzwater, S.E., Jones, J.L., Tozzi, S., Koblizek, M., Roberts, A.E., Herndon, J.,
583 Brewster, J., Ladizinsky, N., Smith, G., Cooper, D., Timothy, D., Brown, S., Selph, K.E.,
584 Sheridan, C.C., Twining, B.S. and Johnson, Z.I.: Southern Ocean Iron Enrichment
585 Experiment: carbon cycling in high- and low-Si waters, *Science*, 304, 5669, 408-414,
586 doi:10.1126/science.1089778, 2004.

587 de Baar, H.J.W., Boyd, P.W., Coale, K.H., Landry, M.R., Tsuda, A., Assmy, P., Bakker,
588 D.C.E., Bozec, Y., Barber, R.T., Brzezinski, M.A., Buesseler, K.O., Boyé, M., Croot, P.L.,
589 Gervais, F., Gorbunov, M.Y., Harrison, P.J., Hiscock, W.T., Laan, P., Lancelot, C., Law,
590 C.S., Levasseur, M., Marchetti, A., Millero, F., Nishioka, J., Nojiri, Y., van Oijen, T.,
591 Riebesell, U., Rijkenberg, M.J.A., Saito, H., Takeda, S., Timmermans, K.R., Veldhuis,
592 M.J.W., Waite, A.M. and Wong, C.-S.: Synthesis of iron fertilization experiments: from the
593 iron age in the age of enlightenment, *Journal of Geophysical Research*, 110, C09S16,
594 doi.10.1029/2004JC002601, 2005.

595 de Baar, H.J.W., de Jong, J.T.M., Bakker, D.C.E., Löscher, B.M., Veth, C., Bathmann, U. and
596 Smetacek, V.: Importance of iron for plankton blooms and carbon dioxide drawdown in the
597 Southern Ocean, *Nature*, 373, 412-415, 1995.

598 de Baar, H.J.W., Buma, A.G.J., Nolting, R.F., Cadee, G.C., Jacques, G., and Treguer, P.J.: On
599 iron limitation of the Southern Ocean: experimental observations in the Weddell and Scotia
600 Seas, *Marine Ecology Progress Series*, 65(2), 105-122, 1990.

601 de Boyer Montégut, C., Madec, G., Fischer, A.S., Lazar, A. and Iudicone, D.: Mixed layer
602 depth over the global ocean: an examination of profile data and a profile-based climatology,
603 *Journal of Geophysical Research*, 109, C12003, doi:10.1029/2004JC002378, 2004.

604 Dehairs, F., Fripiat, F., Cavagna, A.-J., Trull, T.W., Fernandez, C., Davies, D., Roukaerts, A.,
605 Fonseca-Batista, D., Planchon, F. and Elskens, M.: Nitrogen cycling in the Southern Ocean
606 Kerguelen Plateau area: Evidence for significant surface nitrification from nitrate isotopic
607 compositions, *Biogeosciences*, 12, 1459-1482, 2015.

608 Doty, M.S. and Oguri, M.: The island mass effect, *Journal of International Council for*
609 *Exploration of Sea*. 22, 1, 33-37, 1956.

610 Dugdale, R.C. and Goering, J.J.: uptake of new and regenerated form of nitrogen in primary
611 productivity, *Limnology and Oceanography*, 12, 196-206, 1967.

612 Elskens, M., Baeyens, W., Brion, N.N., De Galan, S., Goeyens, L. and de Brauwere, A.:
613 Reliability of N flux rates estimated from ¹⁵N enrichment and dilution experiments in aquatic
614 systems, *Global Biogeochemical Cycles*, 19, GB4028, doi:10.1029/2004GB002332, 2005.

615 Elskens, M., Baeyens, W. and Goeyens, L.: Contribution of nitrate to the uptake of nitrogen
616 by phytoplankton in an ocean margin environment, *Hydrobiologia*, 353, 139-152, 1997.

617 Eppley, R.W. and Peterson, B.J.: Particulate organic matter flux and planktonic new
618 production in the deep ocean, *Nature*, 282, 677-680, 1979.

619 Eppley, R.W.: Temperature and phytoplankton growth in the sea, *Fishery Bulletin*, 70(4),
620 1063-1085, 1972.

621 Falkowski, P.G., Barber, R.T. and Smetacek, V.: Biogeochemical controls and feedbacks on
622 ocean primary production, *Science*, 281, 200-206, 1998.

623 Falkowski, P.G. and Raven, J.A.: The efficiency of photochemistry *in* Chapter 3 The
624 photosynthetic light reactions, p. 92 in *Aquatic Photosynthesis*, eds. Blackwell Science, 375
625 pp., 1997.

626 Franck, V.M., Brzezinski, M.A., Coale, K.H. and Nelson, D.M.: Iron and silicic acid
627 concentrations regulate Si uptake north and south of the Polar Frontal Zone in the Pacific
628 sector of the Southern Ocean, *Deep-Sea Research Part 2*, 47, 15-16, 3315-3338,
629 doi:10.1016/S0967-0645(00)0007-09, 2000.

630 Fripiat, F., Elskens, M., Trull, T.W., Blain, S., Cavagna, A.-J., Fernandez, C., Fonseca-
631 Batista, D., Planchon, F., Raimbault, P., Roukaert, A., and F. Dehairs, F.: Significant mixed
632 layer nitrification in a natural iron-fertilized bloom of the Southern Ocean, in review, *Global*
633 *Biogeochemical Cycles*, in revision (2015).

634 Gall, M.P., Strzepek, R., Maldonado, M., and Boyd, P.: Phytoplankton processes. Part 2:
635 Rates of primary production and factors controlling algal growth during the Southern Ocean
636 Iron Release Experiment (SOIREE), *Deep-Sea Research Part II*, 48, 2571-2590, 2001.

637 Gervais, F., Riebesell, U. and Gorbunov, M.Y.: Changes in Primary Productivity and
638 Chlorophyll a in response to iron fertilization in the Southern Polar frontal zone, *Limnology*
639 *and Oceanography*, 47(5), 1324-1335, 2002.

640 Georges, C., Monchy, S., Genitsaris, S., and Christaki, U.: Protist community composition
641 during early phytoplankton blooms in the naturally iron-fertilized Kerguelen area (Southern
642 Ocean). *Biogeosciences*, 11, 5847-5863, 2014.

643 Gille, S.T., Carranza, M.M., Cambra, R., and Morrow, R.: Wind-induced upwelling in the
644 Kerguelen Plateau Region, *Biogeosciences*, 11, 8373-8397, 2014.

645 Glibert, P.M., Lipschultz, F., McCarthy, J.J. and Altabet, M.A.: Isotope dilution models of
646 uptake and remineralization of ammonium by marine plankton, *Limnology and*
647 *Oceanography*, 27(4), 639-650, 1982.

648 Hagopian, D.S. and Riley, J.G.: A closer look at the bacteriology of nitrification, *Aquacultural*
649 *Engineering*, 19, 223-244, 1998.

650 Heywood, K.J., Barton, E.D. and Simpson, J.H.: The effects of flow disturbance by an
651 oceanic island, *Journal of Marine Research*, 48, 55-73, 1990.

652 Holmes, R.H., Aminot, A., K erouel, R., Hooker, B.A. and Peterson, B.J.: A simple and
653 precise method for measuring ammonium in marine and freshwater ecosystems, *Canadian*
654 *Fisheries and Aquatic Sciences*, 56(10), 1801-1808, 1999.

655 Hutchins, D.A. and Bruland, K.W.: Iron-limited diatom growth and Si:N uptake ratios in a
656 coastal upwelling regime, *Nature*, 393, 561-564, doi:10.1038/31203, 1998.

657 Jochem, F.J., Mathot, S. and Qu eguiner, B.: Size-fractionated primary production in the open
658 Southern Ocean in austral spring, *Polar Biology*, 15, 381-392, 1995.

659 Jacquet, S.H.M., Dehairs, F., Lefèvre, D., Cavagna, A.-J., Planchon, F., Christaki, U., Monin,
660 L., André L., Closset, I. and Cardinal, D.: Early spring mesopelagic carbon remineralization
661 and transfer efficiency in the naturally iron-fertilized Kerguelen area, *Biogeosciences*, 12,
662 1713-1731, 2015.

663 Jacquet, S.H.M., Dehairs, F., Savoye, N., Obernosterer, I., Christaki, U., Monnin, C. and
664 Cardinal, D. : Mesopelagic organic carbon remineralization in the Kerguelen Plateau region
665 tracked by biogenic particulate Ba, *Deep-Sea Research Part 2*, 55, 868-879, 2008.

666 Korb, R.E., Whitehouse, M.J., Thorpe, S.E. and Gordon, M.: Primary production across the
667 Scotia Sea in relation to the physico-chemical environment, *Journal of Marine System*, 57,
668 231-249, 2005.

669 Laws, E., Sakshaug, E., Babin, M., Dandonneau, Y., Falkowski, P., Geider, R., Legendre, L.,
670 Morel, A., Sondergaard, M., Takahashi, M., Williams, P.J.: Photosynthesis and Primary
671 productivity in marine ecosystems: Practical aspects and application of techniques, *Joint*
672 *Global Ocean Flux Study – JGOFS – Report No. 36*, 2002.

673 Lefèvre, D., Guigue, C. and Obernosterer, I.: The metabolic balance at two contrasting sites in
674 the Southern Ocean: The iron fertilized Kerguelen area and HNLC waters, *Deep Sea Research*
675 *Part 2*, 55, 766-776, 2008.

676 Le Quéré, C., Rödenbeck, C., Buithenhus, E.T., Conway, T.J., Langenfelds, R., Gomez, A.,
677 Labuschagne, C., Ramonet, M., Nakazawa, T., Metz, N., Gillett, N. and Heinmann, M.:
678 Saturation of Southern Ocean CO₂ sink due To recent climate change, *Science*, 316(5832),
679 1735, doi:10.1126/science.1136188, 2007.

680 Lipschultz, F., Wofsy, S.C., Ward, B.B., Codispoti, L.A., Friedrich, G. and Elkins, J.W.:
681 Bacterial transformations of inorganic nitrogen in the oxygen-deficient waters of the Eastern
682 Tropical South Pacific Ocean. *Deep-Sea Research Part II*, 37(10), 1513-1541, 1991.

683 Löscher, B.M., de Jong, J.T.M., de Baar, H.J.W., Veth, C. and Dehairs, F.: The distribution of
684 Fe in the Antarctic Circumpolar Current, *Deep Sea Research Part II*, 44, 143-188, 1997.

685 Lucas, M.I., Seeyave, S., Sanders, R., Moore, C.M., Williamson, R. and Stinchcombe, M.:
686 Nitrogen uptake responses to a naturally iron-fertilized phytoplankton bloom during the
687 2004/2005 CROZEX study, *Deep-Sea research Part 2*, 54, 2138-2173, 2007.

688 Malits, A., Christaki, U., Obernosterer, I. and Weinbauer, M.G.: Enhanced viral production
689 and virus-mediated mortality of bacterioplankton in a natural iron-fertilized bloom event
690 above the Kerguelen Plateau, *Biogeosciences*, 11, 6841-6853, 2014.

691 Marra, J.F., Lance, V.P., Vaillancourt, R.D. and Hargreaves, B.R.: Resolving the ocean's
692 euphotic zone, *Deep Sea Research Part I*, 83, 45-50, 2014.

693 Martin, J.H.: Glacial interglacial CO₂ change: the iron hypothesis, *Paleoceanography*, 5, 1-13,
694 1990.

695 Mongin, M., Molina, E. and Trull, T.W.: Seasonality and scale of the Kerguelen plateau
696 phytoplankton bloom: A remote sensing and modeling analysis of the influence of natural
697 iron fertilization in the Southern Ocean, *Deep-Sea Research Part II*, 55, 880-892, 2008.

698 Mosseri, J., Quéguiner, B., Armand, L. and Cornet-Barthaux, V.: Impact of iron on silicon
699 utilization by diatoms in the Southern Ocean: a case study of Si/N cycle decoupling in a
700 naturally iron enriched area, *Deep-Sea Research Part II*, 55, 801-819, 2008.

701 Mulholland, M. R. and Lomas, M.W.: N-uptake and assimilation, pp. 303-384. *In*: Capone,
702 D. G., D. A. Bronk, M. R. Mulholland and E. J. Carpenter (eds.), *Nitrogen in the Marine*
703 *Environment*. Elsevier/Academic, 2008.

704 Nelson, D.M. and Goering, J.J.: A stable isotope tracer method to measure silicic acid uptake
705 by marine phytoplankton, *Analytical Biogeochemistry*, 78, 139-147, 1977a.

706 Nelson, D.M. and Goering, J.J.: Near surface silica dissolution in the upwelling region off
707 northwest Africa, *Deep Sea Research*, 24, 65-73, 1977b.

708 Newel, S.E., Babbitt, A.R., Jayakumar, A. and Ward, B.B.: Ammonia oxidation rates and
709 nitrification in the Arabian Sea, *Global Biogeochemical Cycles*, 25, GB4016,
710 doi:10.1029/2010GB003940, 2011.

711 Obernosterer, I., Christaki, U., Lefèvre, D., Catala, P., Van Wambeke, F. and Lebaron, P.:
712 Rapid bacterial mineralization of organic carbon produced during a phytoplankton bloom
713 induced by natural iron fertilization in the Southern Ocean, *Deep-Sea Research Part II*,
714 *Topical Studies in Oceanography*, 55, 777-789, doi:10.1016/j.dsr2.2007.12.005, 2008.

715 Olson, R.J.: ¹⁵N tracer studies of the primary nitrite maximum, *Journal of Marine Research*,
716 39(2), 203-238, 1981.

717 Park, Y.-H., Durand, I., Kestenare, E., Rougier, G., Zhou, M., d'Ovidio, F., Cotté, C. and Lee,
718 J.H.: Polar Front around the Kerguelen Islands: an up-to-date determination and associated
719 circulation of surface/subsurface waters, *Journal of Geophysical Research: Oceans*, 119,
720 6575-6592, doi:10.1002/2014JC010061, 2014.

721 Park, Y.-H., Roquet, F., Durand, I. and Fuda, J.-L.: Large-scale circulation over and around
722 the Northern Kerguelen Plateau, *Deep-Sea Research Part II*, 55, 566-581, 2008.

723 Planchon, F., Ballas, D., Cavagna, A.-J., Van der Merwe, P., Bowie, A., Trull, T.W.,
724 Laurenceau, E., Davis, D. and Dehairs, F., Carbon export in the naturally iron-fertilized
725 Kerguelen area of the Southern Ocean using ^{234}Th -based approach, *Biogeosciences*, 12, 3831-
726 3848, 2015.

727 Pollard, R.T., Slater, I., Sanders, R.J., Lucas, M.I., Moore, C.M., Mills, R.A., Statham, P.J.,
728 Allen, J.T., Baker, A.R., Bakker, D.C.E., Charette, M.A., Fielding, S., Fones, G.R., French,
729 M., Hickman, A.E., Holland, R.J., Hughes, J.A., Jickells, T.D., Lampitt, R.S., Morris, P.J.,
730 Nédélec, F.H., Nielsdottir, M., Planquette, H., Popova, E.E., Poulton, A.J., Read, J.F.,
731 Seeyave, S., Smith, T., Stinchcombe, M., Taylor, S., Thomalla, S., Venables, H.J.,
732 Williamson, R. and Zubkov, M.V.: Southern Ocean deep-water carbon export enhanced by
733 natural iron fertilization, *Nature*, 457, 577-580, doi:10.1038/nature07716, 2009.

734 Pollard, R., Sanders, R., Lucas, M. and Statham, P.: The Crozet natural iron bloom and export
735 experiment (CROZEX), *Deep-Sea Research Part II*, 54, 1905-1914,
736 doi:10.1016/j.dsr2.2007.07.023, 2007.

737 Quéguiner, B.: Iron fertilization and the structure of planktonic communities in high nutrient
738 regions of the Southern Ocean. *Deep-Sea Research Part II*, 90, 43-54
739 doi:10.1016/j.dsr2.2012.07.024, 2013.

740 Quéguiner, B., Tréguer, P., Peeken, I. and Sharek, R.: Biogeochemical dynamics and the
741 silicon cycle in the Atlantic sector of the Southern Ocean during austral spring 1992, *Deep-
742 Sea Research Part 2*, 44, 69-89, 1997.

743 Rees, A.P., Owens, N.J.P., Heath, M.R., Plummer, D.H. and Bellerby, R.S.: Seasonal nitrogen
744 assimilation and carbon fixation in a fjordic sea loch, *Journal of Plankton Research*, 17, 1307-
745 1324, 1995.

746 Sackett, O., Armand, L., Beardall, J., Hill, R., Doblin, M., Connelly, C., Howes, J., Stuart, B.,
747 Ralph, P. and Heraud, P.: Taxon-specific response of Southern Ocean diatoms to Fe

748 enrichment revealed by synchrotron radiation FTIR microspectroscopy, *Biogeosciences*, 11,
749 7327-7357, 2014.

750 Sambrotto, R.N. and Mace, B.J.: Coupling of biological and physical regimes across the
751 Antarctic Polar Front as reflected by nitrogen production and recycling, *Deep-Sea Research*
752 *Part II* 47, 3339-3367, 2000.

753 Sanial, V., Van Beek, P., Lansard, B., Souhaut, M., Kestenare, E., d'Ovidio, F., Zhou, M. and
754 Blain, S.: Use of Ra isotopes to deduce rapid transfer of sediment-derived inputs off
755 Kerguelen, *Biogeosciences*, 12, 1415-1430, 2015.

756 Sarmiento, J. L., Gruber, N., Brzezinski, M. A. and Dunne, J. P.: High-latitude controls of
757 thermocline nutrients and low latitude biological productivity. *Nature* 427: 56-60, 2004.

758 Sarthou, G., Vincent, D., Christaki, U., Obernosterer, I., Timmermans, K.R. and Brussaard,
759 C.P.D.: The fate of biogenic iron during phytoplankton bloom induced by natural fertilization:
760 Impact of copepod grazing. *Deep-Sea Research Part II* 55, 734-751, 2008.

761 Sarthou G., Timmermans, K.R., Blain, S. and Tréguer, P.: Growth physiology and fate of
762 diatoms in the oceans: a review, *Journal of Sea Research*, 53, 25-42, 2005.

763 Savoye, N., Trull, T.W., Jacquet, S.H.M., Navez, J. and Dehairs, F.: ^{234}Th -based export fluxes
764 during a natural iron fertilization experiment in the Southern Ocean (KEOPS), *Deep-Sea*
765 *Research Part II*, 55, 841-855, 2008.

766 Savoye, N., Dehairs, F., Elskens, M., Cardinal, D., Kopczynska, E.E., Trull, T.W., Wright, S.,
767 Baeyens, W. and Griffiths, B.F.: Regional variation of spring N-uptake and new production in
768 the Southern Ocean, *Geophysical Research Letters*, 31, L03301, doi:10.1029/2003GL018946,
769 2004.

770 Seeyave, S., Lucas, M.I., Moore, C.M. and Poulton, A.J.: Phytoplankton productivity and
771 community structure across the Crozet Plateau during summer 2004/2005, *Deep-Sea*
772 *Research Part 2*, 54, 2020-2044, doi:10.1016/j.dsr2.2007.06.010, 2007.

773 Sigman, D.M., Casciotti, K.L., Andreani, M., Barford, C., Galanter, M. and Böhlke, J.K.: A
774 bacterial method for the nitrogen isotopic analysis of nitrate in seawater and freshwater.
775 *Analytical Chemistry*, 73, 4145-4153, 2001.

776 Sigman, D. M., Altabet, M.A., McCorkle, D. C., Francois, R. and Fischer, G.: The $\delta^{15}\text{N}$ of
777 nitrate in the Southern Ocean: Consumption of nitrate in surface waters, *Global*
778 *Biogeochemical Cycles*, 13(4), 1149-1166, 1999.

779 Slawyk, G., Coste, B., Collos, Y. and Rodier, M.: Isotopic and enzymatic analyses of
780 planktonic nitrogen in the vicinity of Cape Sines (Portugal) during weak upwelling activity,
781 *Deep-Sea Research Part I*, 44, 1-25, 1997.

782 Smetacek, V., Klaas, C., Strass, V.H., Assmy, P., Montresor, M., Cisewski, B., Savoye, N.,
783 Webb, A., d'Ovidio, F., Arrieta, J.M., Bathmann, U., Bellerby, R., Berg, G.M., Croot, P.,
784 Gonzalez, S., Henjes, J., Herndl, G.J., Hoffmann, L.J., Leach, H., Losch, M., Mills, M.M.,
785 Neill, C., Peeken, I., Röttgers, R., Sachs, O., Sauter, E., Schmidt, M.M., Schwartz, J.,
786 Terbrüggen, A. and Wolf-Gladrow, D.: Deep carbon export from a Southern Ocean iron-
787 fertilized diatom bloom, *Nature*, 487, 313-319, doi:10.1038/nature11229, 2012.

788 Sokolov, S. and Rintoul, S.R.: On the relationship between fronts of the Antarctic
789 Circumpolar Current and surface chlorophyll concentration in the Southern Ocean, *Journal of*
790 *Geophysical Research*, 112, C07030, doi:10.1029/2006JC004072, 2007.

791 Takahashi, T., Sutherland, S.C., Wanninkhof, R., Sweeney, C., Feely, R.A., Chipman, D.W.,
792 Hales, B., Friederich, G., Chavez, F., Sabine, C., Watson, A., Bakker, D.C.E., Schuster, U.,
793 Metzl, N., Yoshikawa-Inoue, H., Ishii, M., Midorikawa, T., Nojiri, Y., Körtzinger, A.,
794 Steinhoff, T., Hoppema, M., Olafsson, J., Arnarson, T.S., Tilbrook, B., Johannessen, T.,
795 Olsen, A., Bellerby, R., Wong, C.S., Delille, B., Bates, N.R. and de Baar, H.J.W.:
796 Climatological mean and decadal change in surface ocean pCO₂ and net sea-air CO₂ flux over
797 global oceans, *Deep-Sea Research Part II*, 56, 554-577, doi:10.1016/j.dsr2.2008.12.009, 2009.

798 Takeda, S.: Influence of iron availability on nutrient consumption ratio of diatoms in oceanic
799 waters, *Nature*, 393, 774-777, doi:10.1038/31674, 1998.

800 Timmermans, K.R., Veldhuis, M.J.W., Laan, P. and Brussaard, C.P.D.: Probing natural iron
801 fertilization near the Kerguelen (Southern Ocean) using natural phytoplankton assemblages
802 and diatom cultures, *Deep-Sea Research Part II*, 55, 693-705, 2008.

803 Van Leeuwe, M.A., Scharek, R., de Baar, H.J.W., de Jong, J.T.M. and Goeyens, L.: Iron
804 enrichment experiments in the Southern Ocean: physiological responses of plankton
805 communities, *Deep-Sea Research Part 2*, 44(1-2), 189-207,
806 doi:10.1016/S0967.0645(96)00069-0, 1997.

807 Waldron, H.N., Attwood, C.G., Probyn, T.A. and Lucas, M.I.: Nitrogen dynamics in the
808 Bellingshausen Sea during the Austral spring of 1992, *Deep-Sea Research Part II*, 42(4-5),
809 1253-1276, 1995.

810 Ward, B. B.: Nitrification. In: *Encyclopedia of Ecology*. Eds. S. E. Jorgensen and B. D. Faith,
811 *Ecological Processes*. Vol 3 of *Encyclopedia of Ecology*, 5 vols. Elsevier, Oxford. Pp. 2511-
812 2518, 2008.

813 Ward, B.B. and Zafiriou, O.C.: Nitrification and nitric oxide in the oxygen minimum of the
814 eastern tropical north pacific, *Deep-Sea Research*, 35(7), 1127-1142, 1988.

815 Yool, A., Martin, A.P., Fernandez, C. and Clark, D.R.: The significance of nitrification for
816 oceanic new production, *Nature*, 447, 999-1002, doi:10.1038/nature05885, 2007.

817

818

819

820

821

822

823

824

825

826

827

828

829

830

831

832

833 Table 1: Mixed layer integrated values for particulate organic C (POC), net primary
 834 production (NPP), ammonium uptake (NH_4^+ upt.), nitrate uptake (NO_3^- upt.), ammonium +
 835 nitrate uptake ($\text{NH}_4^+ + \text{NO}_3^-$ upt.), nitrification (Nitr.), f-ratio, and corrected f-ratio by taking
 836 into account the contribution of nitrification (Yool et al., 2007).

837

838

	date	POC mmol m^{-2}	NPP $\text{mmol m}^{-2} \text{ d}^{-1}$	NH_4^+ upt. $\text{mmol m}^{-2} \text{ d}^{-1}$	NO_3^- upt. $\text{mmol m}^{-2} \text{ d}^{-1}$	$\text{NO}_3^- + \text{NH}_4^+$ upt. $\text{mmol m}^{-2} \text{ d}^{-1}$	nitr.* $\text{mmol m}^{-2} \text{ d}^{-1}$	f ratio no Unit	corr. f ratio no Unit
<i>HNLC reference station</i>									
	R-2	26 Oct. 2011	240,3	13,2	5,1	2,0	7,0	0,3	
<i>Meander station</i>									
	E-1	30 Oct. 2011	436,2	43,5	3,6	8,6	12,2	27,3	0,7
	E-3	4 Nov. 2011	325,8	34,5	2,3	2,1	4,3		0,5
	E4-E	14 Nov. 2011	891,0	86,9	7,4	15,2	22,5	8,8	0,7
	E-5	19 Nov. 2011	465,4	53,4	4,7	12,1	16,8	2,0	0,7
	average		529,6	54,6	4,5	9,5	14,0	12,7	0,6
	sd		248,3	22,9	2,2	5,6	7,7	13,1	0,1
<i>Kerguelen Plateau and margin</i>									
	E4-W	12 Nov. 2011	1276,8	252,8	8,0	41,8	49,8	37,7	0,8
	A3-2	17 Nov. 2011	2146,0	179,9	5,9	33,3	39,2	18,1	0,8
	average		1711,4	216,3	7,0	37,5	44,5	27,9	0,8
	sd		614,7	51,5	1,5	6,0	7,5	13,8	0,0
<i>Polar Front</i>									
	F-L	7 Nov. 2011	1565,9	314,6	17,4	63,5	80,8	0,8	

*Only 5 stations had a sufficient depth resolution to allow an integration to be made

**As the f ratio is giving the proportion of primary production sustained by new nutrients. If 100% of the nutrient are considered as regenerated nutrients (Nitrification > N uptake), then the proportion of new nutrient is zero.

839

840

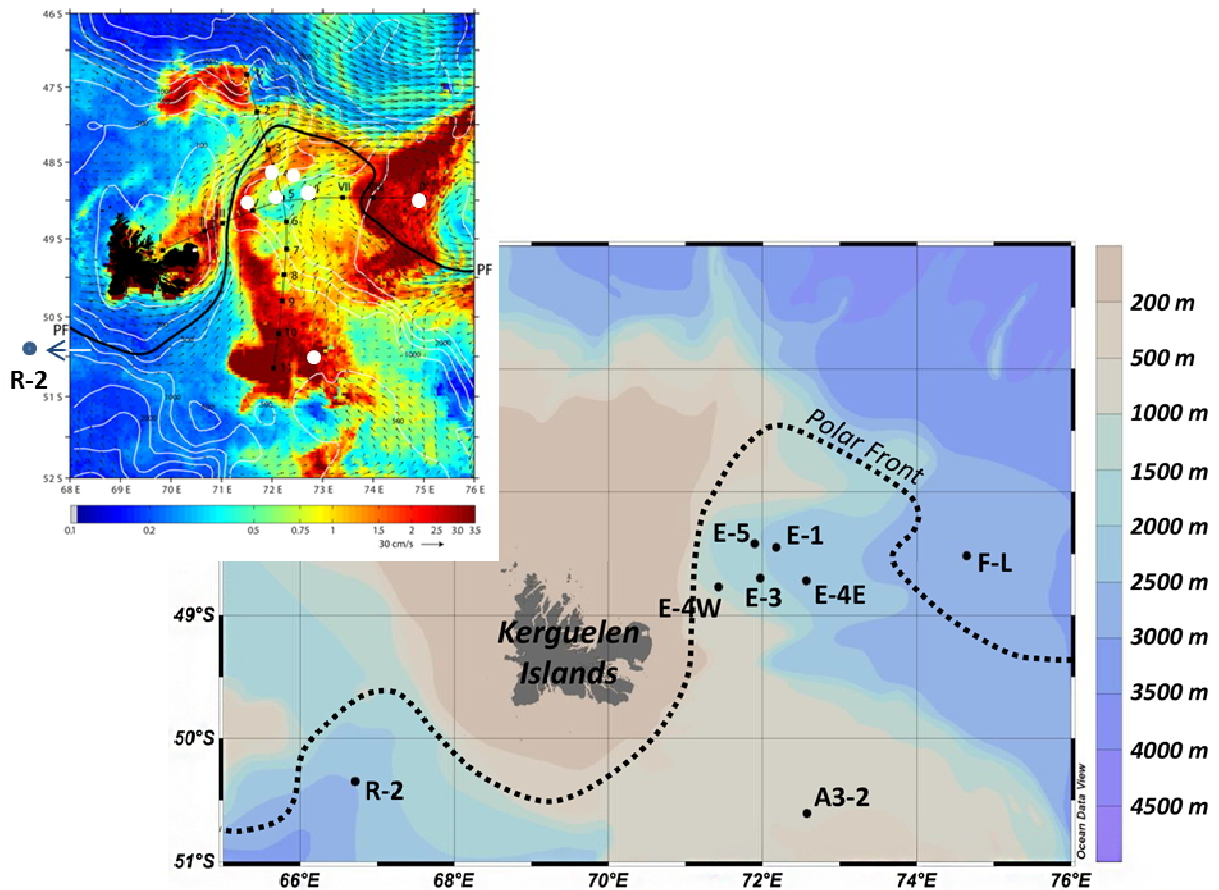
841

842

843 Figure 1: Map of the KEOPS 2 cruise area (Indian sector of the Southern Ocean) showing the
 844 location of stations discussed in the study, courtesy from Ivia Closset. Dotted line represents
 845 the position of the Polar Front from Park et al. (2014). The inset picture gives indication about
 846 surface chl-a (color scale), surface velocity fields (arrows) and the Polar Front (PF, black
 847 line). Black dots in the inset picture represent KEOPS 2 transect stations which were not
 848 concerned by this study; stations for which we performed incubations are represented by the
 849 white circles: the bloom stations over the Kerguelen plateau (E4-W and A3-2) and North of
 850 the Polar Front (F-L); and the meander stations (E stations). The reference HNLC station (R-
 851 2) lays outside the area covered by the map (66.69°E, 50.39°S). This satellite picture
 852 corresponds to the last week of the KEOPS2 cruise. Courtesy of Y. Park and colleagues.

853

854



855

856

857 Figure 2: Nitrate (a), ammonium (b), and nitrite (c) concentration ($\mu\text{mol L}^{-1}$) vs. depth (m).
858 See Annex for detailed $[\text{NH}_4^+]$ vertical profiles and associated Zeu, MLD per station.

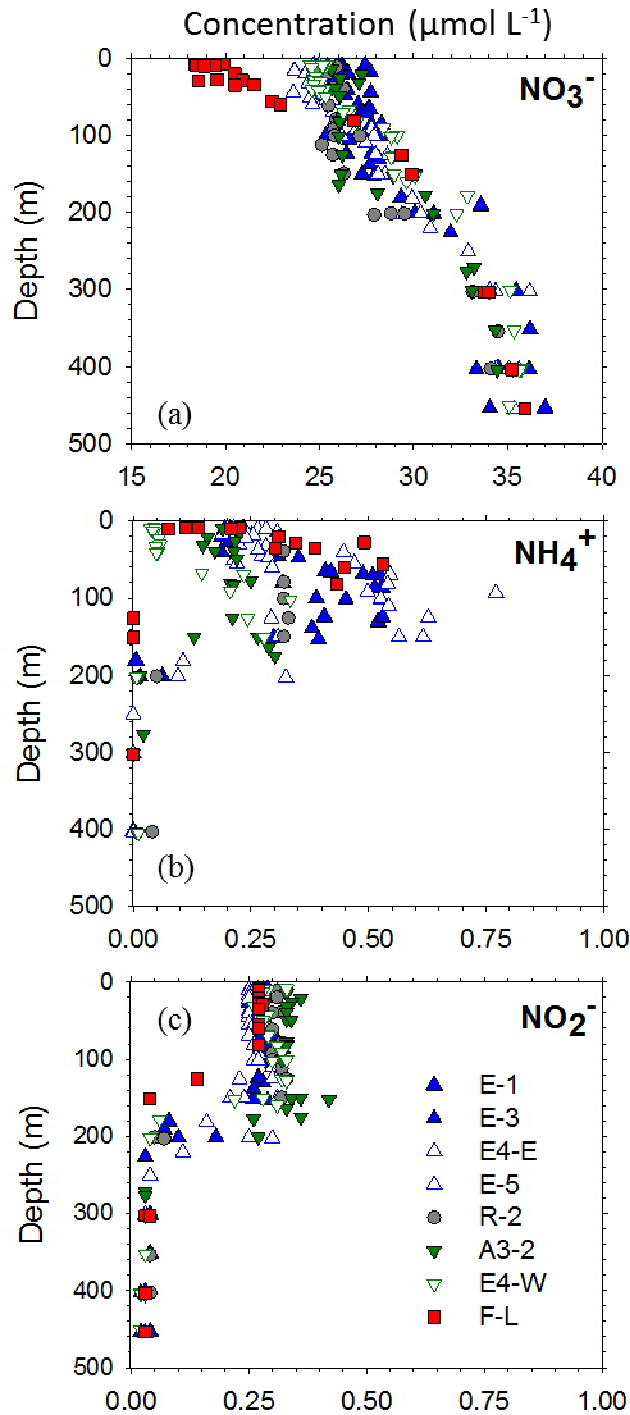
859

860

861

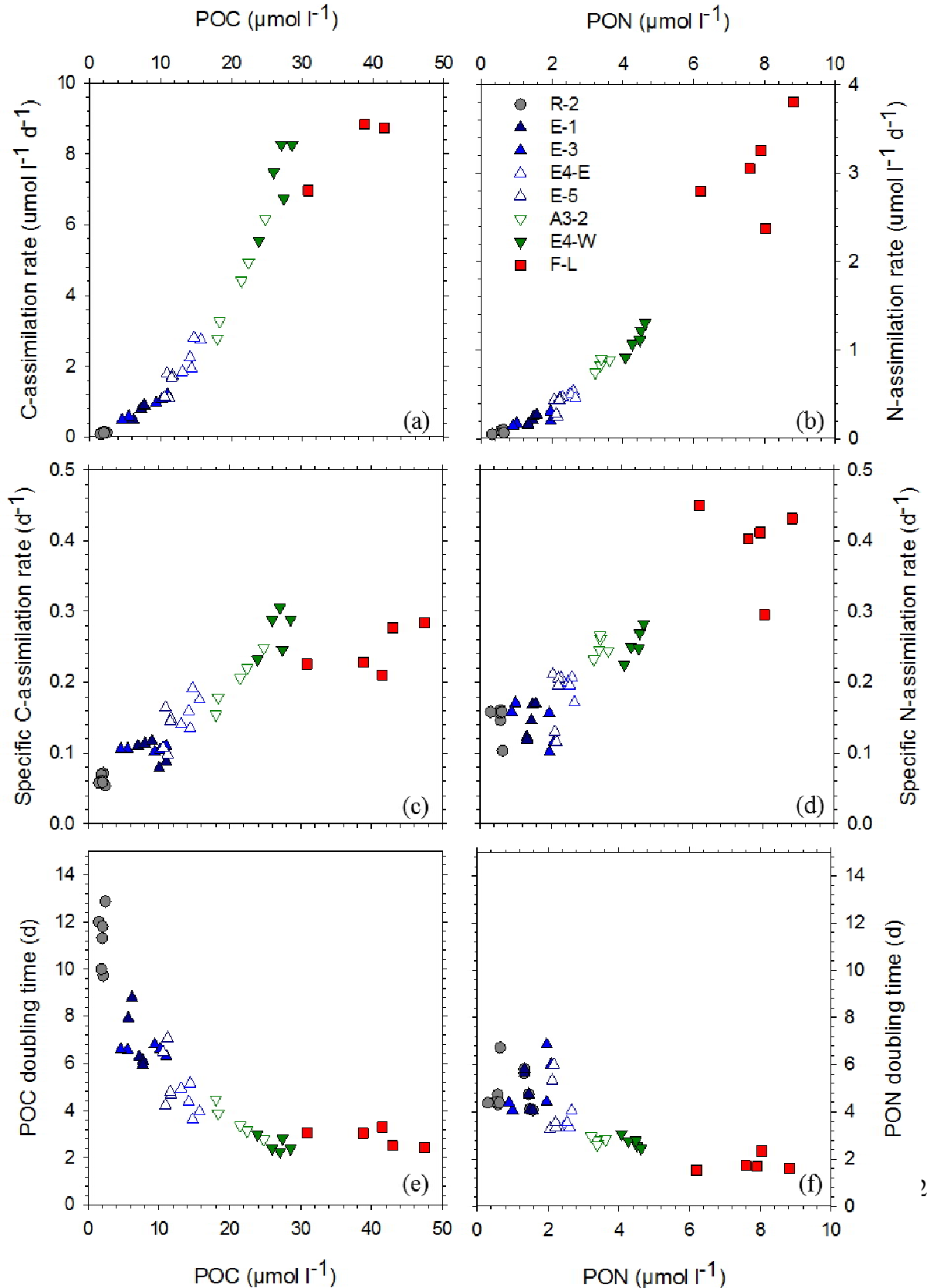
862

863

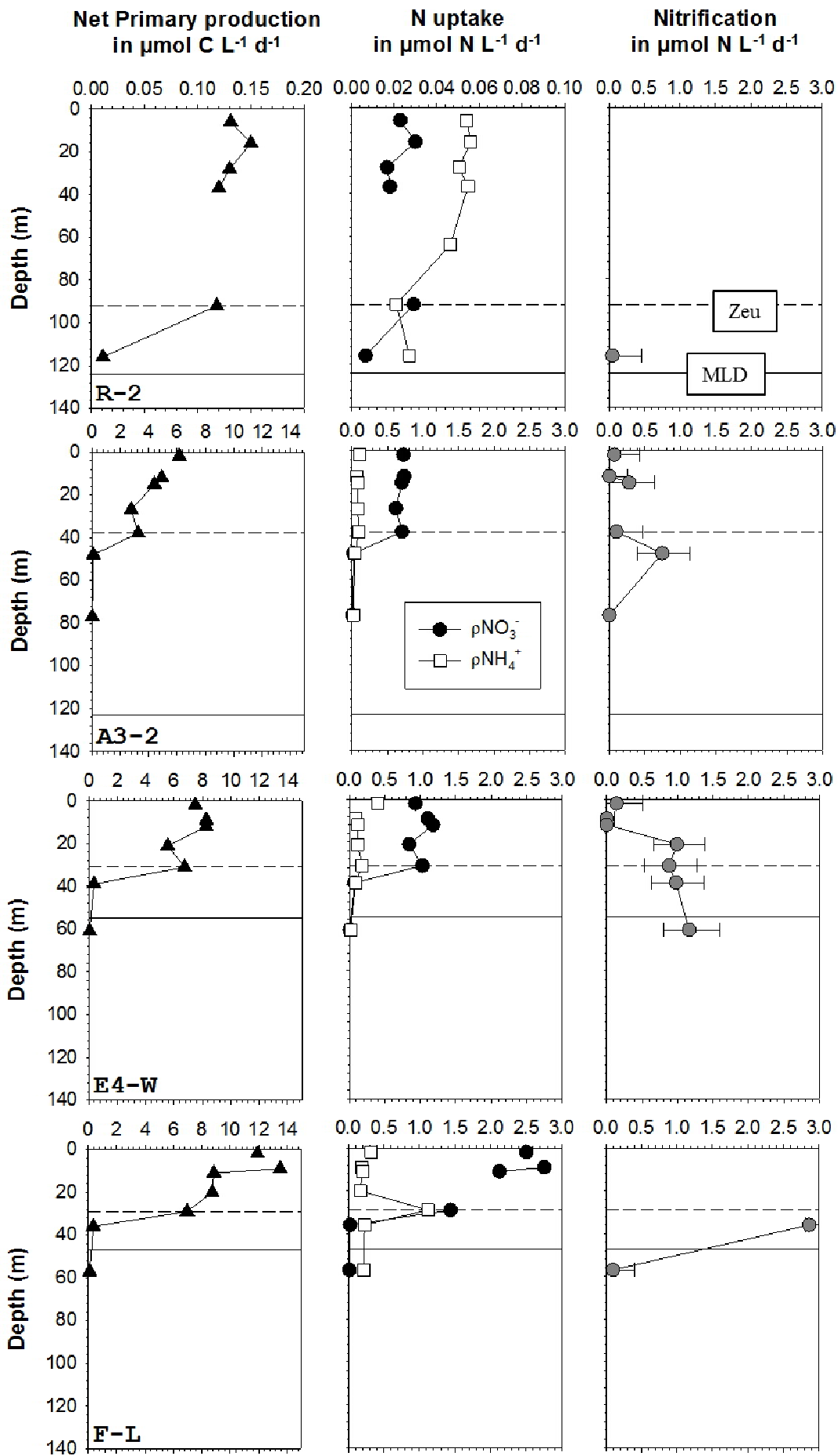


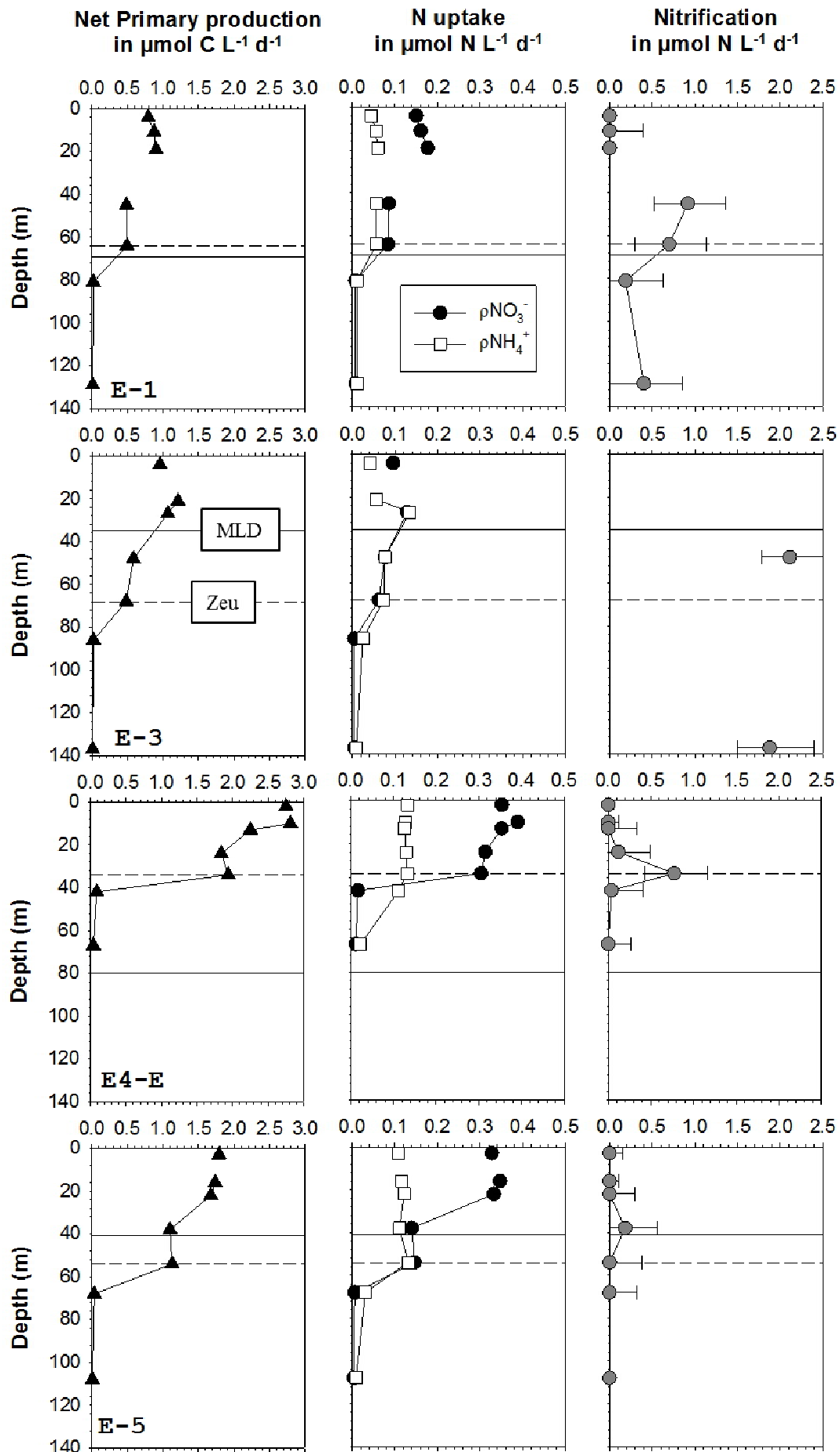
864 Figure 3: Euphotic layer (100 to 1% PAR) relationship between: (a) POC and NPP also called
 865 C-assimilation rate ($\mu\text{mol C m}^{-2} \text{d}^{-1}$); (b) PON ($\mu\text{mol L}^{-1}$) and N-assimilation rates ($\mu\text{mol N m}^{-2}$
 866 d^{-1}); (c) POC and specific C assimilation rate (growth rate; d^{-1}); (d) PON and specific N
 867 assimilation rate (growth rate; d^{-1}); (e) POC and POC doubling time; (f) PON and PON
 868 doubling time.

869



870 Figure 4: Vertical distribution of Net Primary Production NPP (left column), N-uptake
871 (middle column), and nitrification (right column; error bar corresponding to the 5 and 95%
872 percentiles) rates between stations (rows). Note that there is a change of scale between
873 reference R-2 site, high productivity sites (A3-2, F-L, E4-W) and meander sites (E1, E3, E4-
874 E, E5). The dashed line represents the euphotic layer depth ($Z_{eu} = 1\%$ PAR attenuation) and
875 the full line represents the mixed layer depth.





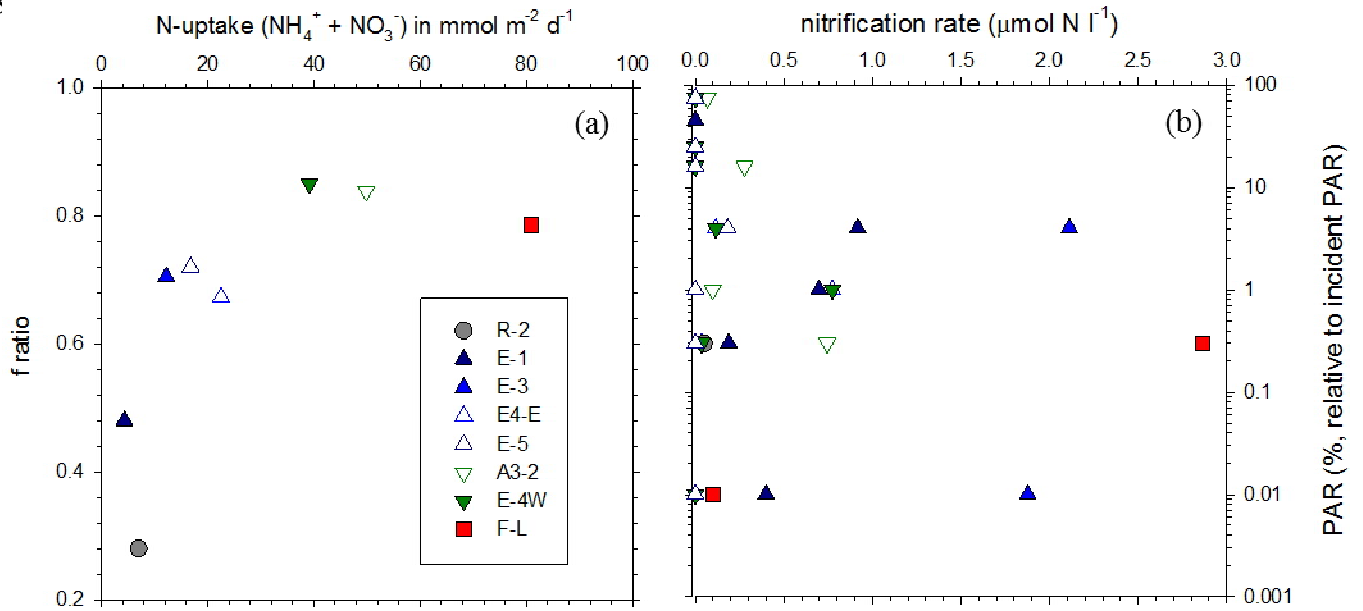
879 Figure 5: Relationship between mixed layer depth integrated N-uptake ($\text{NH}_4^+ + \text{NO}_3^-$) and f-
880 ratio (a), and between PAR (%) and nitrification rates (b).

881

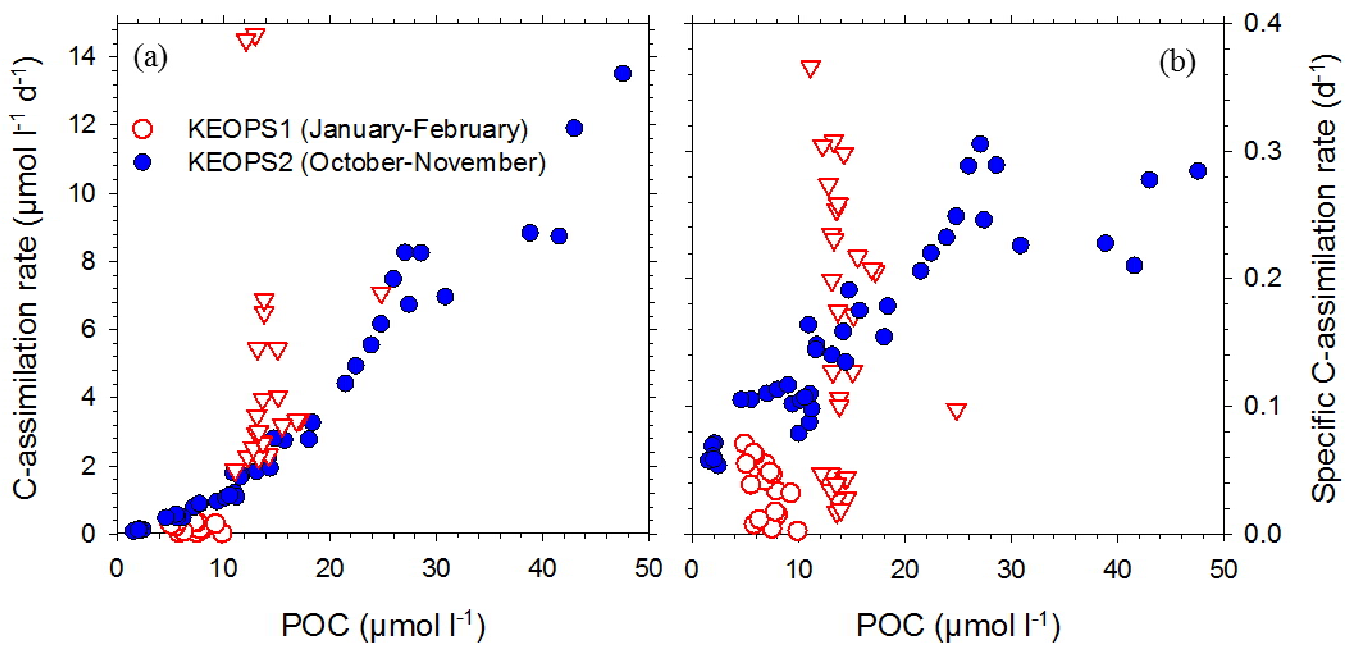
882

883

88



885 Figure 6: Relationship in the euphotic layer (100 to 1% PAR) between biomass (POC) and net
 886 primary production (a), and specific C assimilation rates (growth rate) (b). The KEOPS2
 887 stations are represented in blue, with the circles for the HNLC station (R-2), the normal
 888 triangles for the meander stations (E1 to E5), the inversed triangles for the plateau stations
 889 (A3-2 and E4-W), and the squares for the station north of the Polar Front (F-L). The KEOPS1
 890 stations are in red (Raimbault, KEOPS 1 database). Inversed red triangles represent the
 891 stations over the Kerguelen Southeast Plateau, the red circles the HNLC area east of the
 892 plateau (not sampled during KEOPS2).



893

894